Stem Cell Research & Therapy

RESEARCH

Open Access

Fascia-derived stem cells enhance fat graft retention by promoting vascularization through the HMOX1-HIF-1α pathway

Guo Chen[1†], Jie Long[1,2†], Yuge Zhang[1], Xuhua Zhou[1], Botao Gao[1], Zijin Qin[1,3], Yuhan Zhu[1], Binyu Song[1], Ziwei Cui[1], Zhangzi liu[1], Man Xu[1], Zhou Yu[1*], Baoqiang Song[1*] and Ziang Zhang[1*]

Abstract

Background Adipose tissue is a widely used autologous soft tissue filler in plastic surgery, particularly for volumetric restoration in cases of soft tissue deficiency. However, effectively controlling the retention rate of transplanted fat remains a major challenge. Therefore, this study aims to explore strategies to enhance fat graft retention. We isolated fascia-derived stem cells (FDSCs) from human superficial fascia and compared their gene expression profiles with those of adipose-derived stem cells (ADSCs). Through bioinformatics analysis and functional experiments, we identified significant differences in the angiogenic potential of the two cell types. Based on sequencing results, we further investigated the roles of hypoxia-inducible factor-1α (HIF-1α) and heme oxygenase-1 (HMOX1). This study highlights the critical potential of FDSCs in improving fat graft retention and promoting angiogenesis, offering new strategies for enhancing graft survival and optimizing tissue regeneration therapies.

Methods We isolated fascia-derived stem cells (FDSCs) from human superficial fascia and compared them with adipose-derived stem cells (ADSCs). RNA sequencing was performed to analyze gene expression profiles, followed by bioinformatics analysis to identify differences in angiogenic potential. Functional experiments were conducted to investigate the roles of HIF-1α and HMOX1 in angiogenesis.

Results RNA sequencing revealed significant gene expression differences related to angiogenesis in FDSCs. The expression levels of HMOX1, HIF-1α, and VEGFa were significantly higher in FDSCs than in ADSCs, and HMOX1 positively regulated the expression of HIF-1α and VEGFa. In vitro experiments demonstrated that FDSCs promoted angiogenesis more effectively than ADSCs. In vivo co-transplantation experiments further confirmed that FDSCs improved fat graft retention and vascularization.

†Guo Chen and Jie Long contributed equally and are co- first authors.

*Correspondence:
Zhou Yu
yz20080512@163.com
Baoqiang Song
songbq2012@163.com
Ziang Zhang
zhang_ziang@hotmail.com

Full list of author information is available at the end of the article

© The Author(s) 2025. **Open Access** This article is licensed under a Creative Commons Attribution-NonCommercial-NoDerivatives 4.0 International License, which permits any non-commercial use, sharing, distribution and reproduction in any medium or format, as long as you give appropriate credit to the original author(s) and the source, provide a link to the Creative Commons licence, and indicate if you modified the licensed material. You do not have permission under this licence to share adapted material derived from this article or parts of it. The images or other third party material in this article are included in the article's Creative Commons licence, unless indicated otherwise in a credit line to the material. If material is not included in the article's Creative Commons licence and your intended use is not permitted by statutory regulation or exceeds the permitted use, you will need to obtain permission directly from the copyright holder. To view a copy of this licence, visit http://creativecommons.org/licenses/by-nc-nd/4.0/.

Conclusions We demonstrated that FDSCs can more effectively promote vascularization both in vitro and in vivo, and significantly improve graft retention, indicating their broad potential for future applications in tissue repair and regeneration.

Keywords Superficial Fascia, Stem cells, Vascularization, Graft Retention, HMOX1, HIF-α

Background

Adipose tissue is the most commonly used autologous soft tissue filler in plastic surgery, frequently employed for volumetric restoration in cases of soft tissue deficiency throughout the body. Once transplanted, adipose tissue can remain permanently in the body if it survives. However, controlling the retention rate of transplanted fat remains challenging, posing a significant obstacle to its broader clinical use [1]. Therefore, it is both necessary and urgent to explore methods to enhance the retention of adipose tissue.

Exploring the physiological, biochemical, and structural aspects of adipose tissue is crucial for uncovering its functional characteristics and identifying potential intervention strategies. During early development in organisms, mesenchymal stem cells (MSCs) from the mesoderm differentiate into preadipocytes under the influence of transcription factors such as PPARγ and C/EBPα. These preadipocytes gradually accumulate lipid droplets within their cytoplasm and mature into adipocytes [2]. Simultaneously, some MSCs that highly express Twist1 secrete abundant extracellular matrix components, such as collagen and elastin, forming dense fibrous networks [3, 4]. These networks are continuously remodeled under the influence of mechanical forces and various signaling pathways (such as TGF-β, Wnt/β-catenin, and integrin-mediated signaling), eventually forming fascia that envelops and supports the adipose tissue [5]. In this context, some partially differentiated MSCs reside within the fascia and adipose tissue, playing a role in regulating the development of these tissues. The homology between these tissues suggests that their functions can influence one another.

In the study by Zhang et al., an analysis of the superficial fascia in rats revealed a high concentration of mesenchymal stem cells [6]. These cells can differentiate into functional adipocytes both in vivo and in vitro, actively participating in the regeneration of adipose tissue. Furthermore, Estève et al. [7] have identified stem cells in the fascial interstitium that regulate the dynamic balance of adipose tissue by limiting adipocyte proliferation and promoting the renewal of mature adipocytes. The strong correlation and cellular complementarity between the stem cells in the fascia and those in adipose tissue provide essential support for the development and repair of adipose tissue, positioning the fascia not merely as a mechanical support structure but as a regulatory tissue with significant research potential in the field of adipose tissue regeneration [8–10].

In the early stages of fat transplantation, the transplanted area often becomes hypoxic due to the delayed establishment with the recipient site. In this hypoxic environment, stem cells are actively recruited to rapidly establish the necessary blood supply, a process primarily driven by hypoxia-inducible factors (HIF) [11, 12]. HIF is a transcription factor that stabilizes and activates under low oxygen conditions, promoting the expression of various angiogenic factors, including vascular endothelial growth factor (VEGF), thereby stimulating the formation of new blood vessels. Additionally, heme oxygenase-1 (HMOX1) plays a key role in angiogenesis. HMOX1 degrades heme into carbon monoxide (CO), iron ions, and biliverdin, with CO promoting vascular relaxation and new blood vessel formation [13]. Studies have suggested that, in certain cell types, HMOX1 may function as a downstream factor of HIF. Recent research has also indicated that HMOX1 may have the potential to negatively regulate HIF [14]. However, the specific roles and interaction mechanisms of these factors in stem cells still require further investigation.

Given the significant role of stem cells in promoting vascularization and improving graft survival, this study isolated mesenchymal stem cells (MSCs) from human superficial fascia and, through a combination of bioinformatics analysis and functional experiments, systematically investigated their mechanisms of action in hypoxic environments. By comparing these cells with adipose-derived mesenchymal stem cells, the study provided an in-depth analysis of the differences in gene expression and angiogenic capacity between the two cell types and explored how these differences influence the survival rate of fat grafts. Furthermore, our research not only enhances the understanding of the roles of HIF-1α and HMOX1 in the regulation of angiogenesis by stem cells, but also offers new strategies and methods to improve the efficacy of tissue regeneration therapies.

Method

Inclusion and exclusion criteria

Fascia samples were obtained from patients undergoing elective plastic surgery at the Department of Plastic and Reconstructive Surgery, Xijing Hospital, the Fourth Military Medical University. The study was approved by the institutional ethics committee (Approval Number: KY20222104-F-2). A total of 10 samples were collected,

including 5 fascia samples and 5 fat samples. Informed consent was obtained from all participants.

Inclusion criteria

1. Patients aged 18–45 years.
2. Undergoing elective abdominoplasty or liposuction.
3. In good general health, with no known systemic diseases or infections.

Exclusion criteria

1. History of systemic diseases such as diabetes, hypertension, or autoimmune disorders.

Separation of the fascia

All fascia samples were obtained from the abdominal walls of adult donors aged between 30 and 50 years. Written informed consent was secured from each donor prior to sample collection. The superficial fascia, positioned between the layers of superficial and deep adipose tissue, was exposed following the surgical removal of the deep fat. This fascia was carefully isolated using surgical forceps and excised with scissors to minimize residual adipose tissue. Immediately after excision, the samples were immersed in sterile phosphate-buffered saline (PBS) to preserve them for subsequent experimental analysis.

Quantification of stromal vascular fraction (SVF) cells

We isolated stromal vascular fraction (SVF) cells from fascia and adipose tissue using collagenase digestion, followed by red blood cell lysis. After collagenase treatment, the cell suspension was subjected to centrifugation to separate the SVF cells. The supernatant was discarded, and the resulting cell pellet was resuspended in 1 mL PBS. The number of cells was then quantified using a hemocytometer.

Isolation of FDSC/ADSC

Fascia or adipose tissue was finely minced and digested with 0.8 mg/ml type I collagenase in DMEM at 37 °C, with shaking at 120 rpm for 1 h. The digested mixture was then filtered through a 100-mesh steel sieve and centrifuged at 1,000 g for 10 min. The resulting FDSCs/ADSCs pellets were collected and cultured in high-glucose DMEM (4.5 g/l) supplemented with 10% FBS. The cultures were maintained at 37 °C in a humidified 5% CO2 environment. FDSC/ADSC reached confluence after 1 week of culture, with the medium refreshed every 2 days.

Differentiation of FDSC/ADSC into adipocytes, osteoblasts, and chondrocytes

FDSC/ADSC were seeded in 6-well plates and cultured until adherence. Adipogenic, osteogenic, and chondrogenic differentiation of FDSCs/ADSCs was induced using specific differentiation kits: the Adipogenic Differentiation Kit (Oricell-HUXMD-90031), Osteoblast Differentiation Kit (Oricell-GUXMD-90021), and Chondrogenic Differentiation Kit (Oricell-GUXMD-90041). On day 21 of induction, cells were fixed with paraformaldehyde. The medium was replaced every three days throughout the differentiation process.

Flow cytometry

Flow cytometry was performed on Fascia-Derived Stem Cells (FDSCs) and Adipose-Derived Stem Cells (ADSCs) isolated from fascia and adipose tissues. Initially, cell suspensions from FDSCs and ADSCs were washed once with PBS and centrifuged for 5 min at 700 g and 900 g, respectively. The pellets were then resuspended in PBS, washed again, and centrifuged to prepare for antibody labeling. For immunophenotyping, the pellets were incubated for 20 min at 4 °C in the dark with fluorochrome-conjugated monoclonal antibodies from Biolegend: CD31-PE (303105), CD34-FITC (343603), and CD45-APC (304037). After incubation, cells were centrifuged and resuspended in stain buffer (BD Biosciences). For each sample, 100,000 events were acquired using a BD Accuri C6 flow cytometer (BD Biosciences). The flow cytometry analyses were conducted using FlowJo software version 10.8.

RNA isolation, quantifcation and quantitative realtime PCR (qPCR)

FDSCs (Fascia-Derived Stem Cells) and ADSCs (Adipose-Derived Stem Cells) isolated from fascial and adipose tissues underwent adipogenic, osteogenic, and chondrogenic induction for a period of 21 days. Following this, the expression levels of genes associated with adipogenesis (PPARγ, FABP4), osteogenesis (RUNX2, BMP-2), and chondrogenesis (SOX9, Type II collage) were quantitatively analyzed using quantitative real-time polymerase chain reaction (qPCR). This technique was utilized to evaluate the differentiation efficiency of these cells under specific induction conditions. RNA extraction was conducted using TRIzol reagent. Tissue homogenization was performed by adding TRIzol, followed by the collection of cellular debris. Chloroform was added to the homogenate, and after centrifugation, the aqueous phase was transferred to a new tube. RNA was precipitated by adding isopropanol and centrifuging the mixture. The RNA pellet was washed with 75% ethanol, air-dried, and then resuspended in enzyme-free water.

For cDNA synthesis, a reverse transcription kit (11141ES10, Yeasen) was used. Quantitative real-time PCR was subsequently performed using SYBR Green reagent (11201ES03, Yeasen) and gene-specific primers to quantify gene expression accurately.

The primer sequences for the genes were: Human HIF-1a forward sequence: 5′-AAGTGTACCCTAACTAGCCG-3′, reverse sequence: 5′-CACAAATCAGCACCAAGC-3′. PPARγ forward sequence: 5′-CAAAGTGCAATCAAAGTGG-3′, reverse sequence: 5′-TGAGGGAGTTGGAAGGCT-3′. FABP4 forward sequence: 5′-GGAAAGTCAAGAGCACCA-3′, reverse sequence: 5′-CACCACCAGTTTATCATCCT-3′. RUNX2 forward sequence 5'- AAGTTACAGTAGATGGACCTC-3' reverse sequence:5'- CTCTGTCCTTGTGGATTAA-3'. Type II collage forward sequence: 5'- GCTCCCAGAACATCACCTACC – 3', reverse sequence: 5'- GTGAACCTGCTATTGCCCTCT – 3'. SOX9 forward sequence: 5'- ACCGACCACCAGAACTCC – 3', reverse sequence: 5′-CTGCGGGATGGAAGGGAC-3′. GAPDH forward sequence: 5′-ACAACAGCCTCAAGATCATCAGC-3′, reverse sequence: 5′-GCCATCACGCCACAGTTTCC-3′.

RNA-seq

Total RNA was extracted using the Total RNA Extractor(Trizol)kit (B511311, Sangon, China) according to the manufacturer's protocol, and treated with RNase-free DNase I to remove genomic DNA contamination. RNA integrity was evaluated with a 1.0% agarose gel. Thereafter, the quality and quantity of RNA were assessed using a NanoPhotometer ® spectrophotometer (IMPLEN, CA, USA) and a Qubit®2.0 Flurometer (Invitrogen). The high quality RNA samples were subsequently submitted to the Sangon Biotech (Shanghai) Co., Ltd. for library preparation and sequencing.

Library preparation and sequencing

A total amount of 1 μg RNA per sample was used as input material for the RNA sample preparations. Sequencing libraries were generated using VAHTSTM mRNA-seq V2 Library Prep Kit for Illumina® following manufacturer's recommendations and index codes were added to attribute sequences to each sample. Briefly, mRNA was purified from total RNA using poly-T oligo-attached magnetic beads. Fragmentation was carried out using divalent cations under elevated temperature in VAHTSTM First Strand Synthesis Reaction Buffer (5X). First strand cDNA was synthesized using random hexamer primer and M-MuLV Reverse Transcriptase (RNase H-). Second strand cDNA synthesis was subsequently performed using DNA polymerase I and RNase H. Remaining overhangs were converted into blunt ends via exonuclease/polymerase activities. After adenylation of 3' ends of DNA fragments, adaptor was ligated to prepare for library. In order to select cDNA fragments of preferentially 150 ~ 200 bp in length, the library fragments were purified with AMPure XP system (Beckman Coulter, Beverly, USA). Then 3 μL USER Enzyme (NEB, USA) was used with size-selected, adaptor-ligated cDNA at 37 °C for 15 min followed by 5 min at 95 °C before PCR. Then PCR was performed with Phusion High-Fidelity DNA polymerase, Universal PCR primers and Index (X) Primer. At last, PCR products were purified (AMPure XP system) and library quality was assessed on the Agilent Bioanalyzer 2100 system. The libraries were then quantified and pooled. Paired-end sequencing of the library was performed on the NovaSeq sequencers (Illumina, San Diego, CA).

Data assessment and quality control

FastQC (version 0.11.2) was used for evaluating the quality of sequenced data. Raw reads were filtered by Trimmomatic (version 0.36) according to several steps: 1) Removing adaptor sequence if reads contains; 2) Removing low quality bases from reads 3' to 5' ($Q < 20$); 3) Removing low quality bases from reads 5' to 3' ($Q < 20$); 4) Using a sliding window method to remove the base value less than 20 of reads tail (window size is 5 bp); 5) Removing reads with reads length less than 35 nt and its pairing reads. And the remaining clean data was used for further analysis.

Alignment with reference genome

Clean reads were mapped to the reference genome by HISAT2 (version 2.0) with default parameters. RSeQC (version 2.6.1) was used to statistics the alignment results. The homogeneity distribution and the genome structure were checked by Qualimap (version 2.2.1). BEDTools (version 2.26.0) was used to statistical analysis the gene coverage ratio.

Expression analysis

Gene expression values of the transcripts were computed by StringTie (version 1.3.3b). Principal Component Analysis (PCA) and Principal co-ordinates analysis (PCoA) were performed to reflect the distance and difference between samples. The TPM (Transcripts Per Million), eliminates the influence of gene lengths and sequencing discrepancies to enable direct comparison of gene expression between samples. DESeq2 (version 1.12.4) was used to determine differentially expressed genes (DEGs) between two samples. Genes were considered as significant differentially expressed if q-value ≤ 0.001 and $|FoldChange| \geq 2$. When the normalized expression of a gene was zero between two samples, its expression value was adjusted to 0.01 (as 0 cannot be plotted on a log plot). If the normalized expression of a certain gene in two libraries was all lower than 1, further differential expression analysis was conducted without this gene. Gene expression differences were visualized by scatter plot, MA plot and volcano plot. The transcriptome sequencing data are included in the supplementary materials (Supplementary file 1).

Functional analysis of differentially expressed genes

Functional enrichment analyses including Gene Ontology (GO) was performed to identify which DEGs were significantly enriched in GO terms or metabolic pathways. Gene Ontology (GO) is an international standard classification system for gene function. DEGs are mapped to the GO terms (biological functions) in the database, the number of genes in every term is calculated, and a hypergeometric test is performed to identify significantly enriched GO terms in the gene list out of the background of the reference gene list. GO terms with false discovery rate (q-value) < 0.05 were considered as significantly altered.

Tube formation assay

A Matrigel assay was performed to assess the angiogenic potential of a coculture system consisting of Fascia-Derived Stem Cells (FDSCs), Adipose-Derived Stem Cells (ADSCs), and Human Umbilical Vein Endothelial Cells (HUVECs). Each well of a 24-well plate was coated with 500 µL of Matrigel (Corning, Kaiserslautern, Germany) and allowed to polymerize. Subsequently, 10,000 HUVECs were seeded into each well. A Transwell insert was then placed into the well, containing 10,000 FDSCs/ADSCs, and the setup was incubated for 10 h. Quantitative analysis of angiogenesis was performed using the Angiogenesis Analyzer plugin for ImageJ Version 2 (NIH, Bethesda, MD, USA).

Hypoxia treatment

Cells were transferred to a hypoxia incubator maintained at 1% O_2, 5% CO_2, and 94% N_2 after the hypoxic environment was established and stabilized. To minimize oxygen influx, all manipulations were conducted rapidly and using pre-equilibrated medium under hypoxic conditions.

Induction and inhibition of HMOX1

Following the previously described protocols, FDSCs and ADSCs were cultured under both normoxic conditions (21% O_2) and hypoxic conditions (1% O_2, 5% CO_2, 94% N_2) for 24 h. Subsequently, cells were subjected to drug treatments based on established methodologies from relevant literature. Specifically, cells were treated with 10 µM CP-312 for 2 h [15] and with 20 µM SnPPIX for 24 h [16] under the same conditions. Upon completion of the treatments, cell samples were immediately collected for subsequent analyses. CP-312 and SnPPIX were purchased from TargetMol and prepared according to the manufacturer's instructions.

Lentiviral-mediated knockdown of HMOX1 in FDSCs and ADSCs

Lentiviral vectors used in this study were purchased from GeneCopoeia (Catalog: LPP-CSHCTR001-LVRU6GP-500), pseudotyped with VSV-G protein, driven by the U6 promoter, and containing EGFP as a reporter gene. The vectors also carry a puromycin resistance gene for selection. Polybrene was used as a transduction enhancer at a final concentration of 5–8 µg/ml. The procedure was performed as follows:

24 h before transduction, FDSCs and ADSCs were seeded at 5×10^5 cells per well in a 24-well plate, with 2 ml of DMEM supplemented with 10% heat-inactivated fetal bovine serum (FBS). Cells were incubated at 37 °C with 5% CO_2 until they reached 70–80% confluence. The culture medium was then replaced with 1 ml of lentiviral suspension at MOI of 5, along with 1 ml of DMEM containing 10 µg/ml Polybrene (final concentration). For control wells, only Polybrene-containing medium was added. After viral infection, the cells were incubated for 48 h at 37 °C with 5% CO_2.

Following transduction, the medium was replaced with 2 ml of fresh DMEM containing 10% heat-inactivated FBS (without Polybrene), and cells were incubated for an additional 2 days. After the cells recovered, puromycin selection was initiated by adding 2 µg/ml puromycin in DMEM supplemented with 10% heat-inactivated FBS. The selection medium was replaced every 3–4 days until stable cell colonies were formed. Once the cells reached confluence in the 6-well plate, they were harvested for subsequent experiments.

Stabilizing HIF-1α in FDSCs/ADSCs using FG-4592

FG-4592 (purchased from TargetMol, T2515) was prepared at a concentration of 25 µM [17] in fresh DMEM containing 10% heat-inactivated FBS, following the manufacturer's instructions. The prepared medium was then added to the cultured FDSCs/ADSCs and incubated for 1 day. Cell samples were collected after incubation for subsequent experiments.

H&E staining

For histological analysis, tissues were fixed in a 4% paraformaldehyde solution and embedded in paraffin. Sections of 8 µm thickness were deparaffinized, rehydrated, and then stained with Hematoxylin and Eosin.

Phalloidin immunofluorescence staining

10,000 FDSCs/ADSCs were uniformly seeded onto a coverslip and allowed to adhere for 6 h, covering approximately 50% of the coverslip area. The cells were then fixed with 4% paraformaldehyde for 30 min, followed by three washes with PBS to remove excess paraformaldehyde. Subsequently, the cells were permeabilized

with 0.4% Triton X-100 in PBS at room temperature for 10 min, and washed three times with PBS. Phalloidin solution (Uelandy-YP0052S) was then applied according to the manufacturer's instructions and incubated at room temperature for 20 min to stain the cells. After staining, the coverslips were washed three times with PBS and examined under a fluorescence microscope.

Immunofluorescence staining

Following deparaffinization, antigen retrieval was performed on the paraffin sections. After air-drying, the sections were blocked with 3% BSA for 30 min. The sections were then washed three times with PBST before the addition of the primary antibody (CD31 1:100, HMOX1 1:250, VEGF 1:200). The slides were placed flat in a humidified chamber and incubated overnight at 4 °C. The slides were then washed three times on a shaker in PBST, each for 5 min. The corresponding secondary antibody was added and incubated in the dark at room temperature for 50 min. After incubation, the slides were washed three times on a shaker in PBST, followed by counterstaining with DAPI to label the nuclei. Finally, the slides were washed three more times in PBST, mounted, and observed under a fluorescence microscope to capture images.

Oil Red O staining

After adipogenic induction, the cells were fixed with paraformaldehyde for 30 min and then carefully washed three times with PBS to remove excess paraformaldehyde. The fixed samples were stained with 1 mg/ml Nile Red for 20 min to assess lipid accumulation.

Western blot

The culture medium was discarded from the culture dish, which was then washed three times with PBS. A mixture of RIPA buffer containing 1% protease and phosphatase inhibitors was added, and the dish was placed on ice. The cells were disrupted using a sterile pestle for 3 min, followed by lysis for 30 min. The lysate was collected into an EP tube and centrifuged at 12,000 rpm for 10–20 min at 4 °C, and the supernatant was collected. Protein concentration was determined using the BCA method, after which proteins were denatured by adding loading buffer and boiling in a water bath for 5 min.

Equal amounts of protein were loaded onto SDS-PAGE gels, with the gel concentration selected based on the molecular weight of the target protein (P2011, NCM Biotech, Shanghai, China). The proteins were then electrophoresed and transferred onto PVDF membranes. These membranes were blocked with a TBST solution containing 5% skimmed milk powder for 1 h at room temperature. The PVDF membranes were then washed with TBST and incubated overnight at 4 °C with the following rabbit anti-human primary antibodies: HIF1 (57174-1, Signalway Antibody, 1:1000); HMOX1(32266-1, Signalway Antibody, 1:1000); VEGFa(41552-1, Signalway Antibody, 1:1000);GAPDH, (ab8245,abcam,1:1000). The next day, the membranes were washed with TBST and incubated with Goat anti-rabbit IgG-HRP antibody (CW0103, Sanying, Wuhan, China, 1:5000) for 2 h at room temperature. Protein bands were visualized using an ECL developer (310212, Zeta Life) under a Tanon 4600 instrument.

Adipose transplantation combined with FDSCs

For the fat implantation experiments, a total of 30 nude mice were utilized. These mice were randomly divided into two primary groups:

1. ADSCs + Fat Group: Fat grafts combined with adipose-derived stem cells (ADSCs).
2. FDSCs + Fat Group: Fat grafts combined with fascia-derived stem cells (FDSCs).

Each primary group was further subdivided based on three distinct time points for observation: day 7, day 14, and day 30 post-transplantation. This resulted in six subgroups, with five nude mice ($n = 5$) assigned to each subgroup.

Adipose tissue was obtained via liposuction and placed in a centrifuge tube. The samples were centrifuged at 4 °C and 1000 rpm for 3 min. Following centrifugation, the upper oil layer and lower blood layer were carefully discarded, retaining only the middle layer of adipose tissue. Subsequently, 0.5 ml of the purified adipose tissue was mixed with 1×10^7 FDSCs or ADSCs, depending on the group assignment. This cell-adipose mixture was then transplanted into the dorsal region of each nude mouse using a 1 ml syringe. Throughout the experimental procedures, all possible measures were taken to minimize pain, suffering, and distress in the mice. Prior to the surgical procedures, mice were anesthetized with ketamine to ensure they did not experience pain during the fat graft transplantation. Post-transplantation, samples were collected on days 7, 14, and 30 for subsequent observation and analysis.

Animal characteristics and husbandry conditions

The animals used in the study were nude mice of the BALB/c-nu strain, male, 8 weeks old, and weighed approximately 20 g at the start of the experiment. The nude mice were housed in a specific pathogen-free (SPF) facility, with controlled temperature (22–24 °C), humidity (50–60%), and a 12-hour light/dark cycle. The mice had ad libitum access to standard rodent chow and water, and bedding was changed regularly to maintain a clean environment.

Animal euthanasia

At the conclusion of the experiment, the animals were euthanized using an overdose of pentobarbital sodium administered intraperitoneally. The dosage used was 100 mg/kg to ensure a humane and painless death. Death was confirmed by the absence of a heartbeat and respiratory movement.

Blinding and allocation awareness

At all stages of the experiment, including group allocation, conduct of the experiment, outcome assessment, and data analysis, all participants were aware of the group allocation.

The work has been reported in line with the ARRIVE guidelines 2.0.

Results

Presence of CD34 + cells in the superficial Fascia

The superficial fascia is a continuous layer of dense connective tissue located between the subcutaneous dermis and skeletal muscle (Fig. 1a). This tissue appears white and opaque in the body and is easily separable from both adipose tissue and skeletal muscle (Fig. 1b). Anatomical observations reveal that the superficial fascia has a pale, gelatinous appearance, in sharp contrast to the yellow, soft appearance of adipose tissue (Fig. 1c). H&E staining of the tissue's internal structure shows that adipose tissue is primarily composed of adipocytes, while the superficial fascia consists mainly of microvasculature, abundant collagen, and elastic fibers (Fig. 1d). We also observed smaller adipocytes within the superficial fascia. Comparing the quantity of stromal vascular fraction (SVF) extracted from both fascia and adipose tissue (The details can be found in the Methods section.), we found a significantly higher number of SVF cells in the fascia than in the adipose tissue, with statistical significance ($p < 0.05$, Fig. 1e). Next, we used CD34 immunofluorescence staining to label stem cells (Fig. 1f). The immunofluorescence results showed widespread expression of CD34 + cells in adipose tissue. By quantifying the positive fluorescence area, we observed that the number of CD34 + cells in the superficial fascia slightly exceeded that in adipose tissue (Fig. 1g).

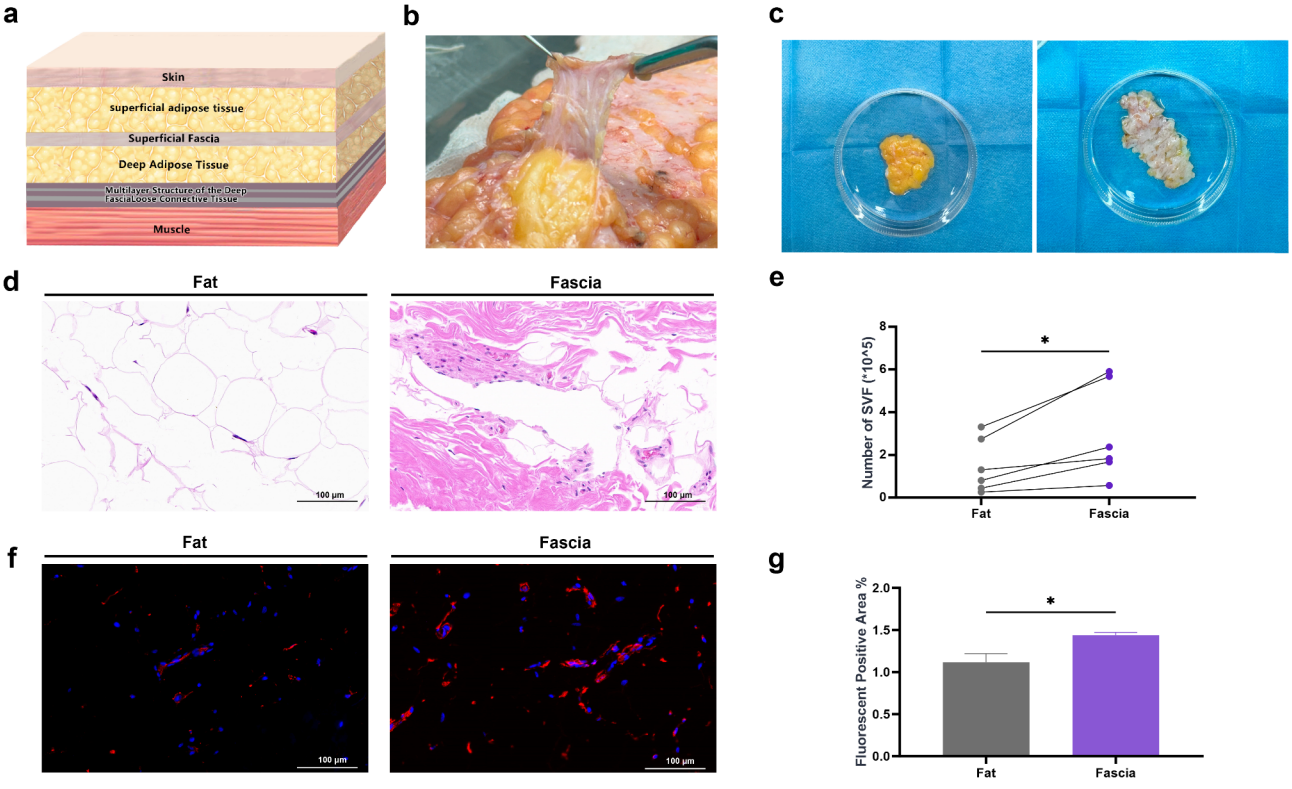

Fig. 1 Morphological Observation and Cytological Analysis of the Superficial Fascia. (**a).** Schematic diagram illustrating the anatomical location of the superficial fascia. (**b).** Gross anatomical structure of the superficial fascia located beneath the abdominal skin. (**c).** Visual comparison of superficial fascia and adipose tissue appearances. (**d).** H&E staining of superficial fascia and adipose tissue. (**e).** A scatter plot depicting the distribution of SVF cell counts in superficial fascia compared to adipose tissue. **(f).** Immunofluorescence staining was performed on superficial fascia and adipose tissue, where CD34 was labeled with red fluorescence and nuclei were counterstained with DAPI in blue. (**g).** A column graph showing the quantification of CD34 fluorescent positive area in superficial fascia and adipose tissue

Differences in stem cells from superficial fascia and adipose tissue

To ensure that the cells used in the experiment were fascia-derived stem cells (FDSCs) and adipose-derived stem cells (ADSCs) rather than other cell types, we cultured the stromal vascular fraction (SVF) from superficial fascia and adipose tissue to passage 3 (P3) and then identified the cells using flow cytometry (Fig. 2a). Flow cytometry analysis revealed that CD34 + cells accounted for 93.13% ± 4.20%, SCA-1 + cells for 99.4% ± 0.80%, and CD29 + cells for 96.8% ± 1.63%, all of which are specific markers for mesenchymal stem cells. Additionally, the cells exhibited minimal expression of FAP- (98.77% ± 0.47%) and CD45- (97.33% ± 0.36%) markers, indicating that they were not fibroblasts or immune cells. Furthermore, CD31- cells were found to be 99.2% ± 0.60%, further confirming the purity of the mesenchymal stem cell population. To account for individual variation, all assays were repeated three times.

In the adipogenic, chondrogenic, and osteogenic differentiation experiments (Fig. 2b), after 21 days of differentiation induction, Oil Red O, Alcian Blue, and Alizarin Red staining were used to evaluate the differentiation outcomes. A significant number of ADSCs differentiated into adipocytes, with bright red lipid droplets stained by Oil Red O, while FDSCs showed a markedly lower adipogenic capacity. Only a few FDSCs differentiated into adipocytes, and those that did typically contained multilocular lipid droplets, which contrasted with the large, unilocular lipid droplets seen in ADSCs. In contrast, quantitative analysis using ImageJ of Alcian Blue-stained glycosaminoglycans (GAGs) and Alizarin Red S-stained calcium deposits indicated that FDSCs exhibited slightly higher chondrogenic and osteogenic differentiation potential compared to ADSCs.

To further validate these findings, we conducted qRT-PCR to analyze the expression of adipogenic-related genes (PPARG, FABP4), chondrogenic-related genes (RUNX2, BMP2), and osteogenic-related genes (SOX9, Type II collagen). (Fig. 2c). The qRT-PCR results showed that the expression of adipogenesis-related genes, such as Pparg and Fabp4, was significantly lower in FDSCs than in ADSCs. On the other hand, osteogenesis-related genes like RUNX2 and BMP2, as well as the

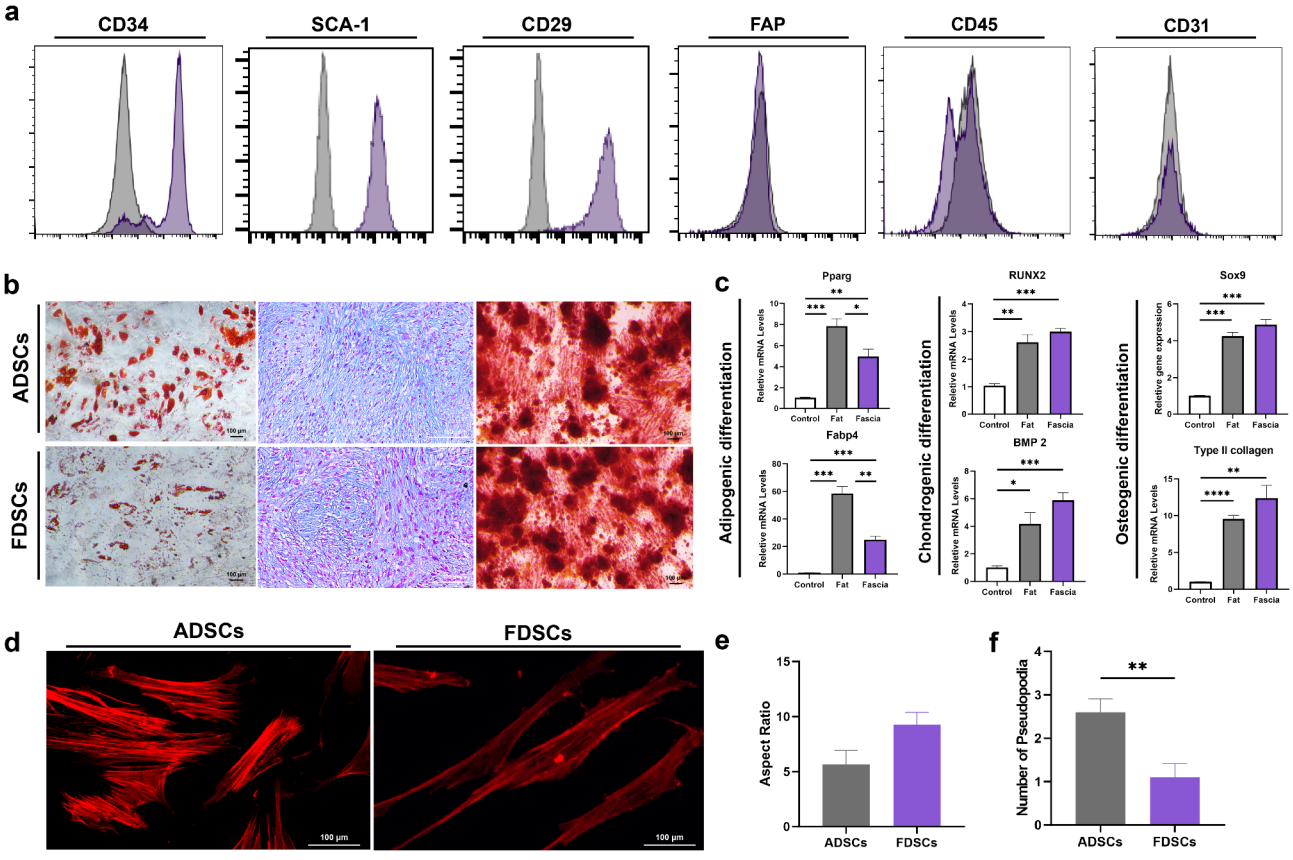

Fig. 2 Characterization and differentiation analysis of SVF, FDSCs, and ADSCs. (**a**) FACS analysis of FDSCs and ADSCs (**b**) Assessment of adipogenic, chondrogenic, and osteogenic differentiation potential of FDSCs and ADSCs (from left to right: Oil Red O staining, Alcian Blue staining, and Alizarin Red S staining). (**c**) qPCR analysis of the expression of genes associated with adipogenic, chondrogenic, and osteogenic differentiation. (**d**) Phalloidin Immunofluorescence Staining of FDSCs and ADSCs. (**e**) (**f**) Quantification of cell aspect ratio and number of pseudopodia from Phalloidin immunofluorescence staining

chondrogenesis-related genes SOX9 and Type II Collagen, were expressed at slightly higher levels in FDSCs compared to ADSCs.

Next, we used phalloidin staining to label intracellular actin and observe the cell morphology (Fig. 2d). The immunofluorescence results revealed that cells from both sources exhibited a spindle shape. However, the cells derived from superficial fascia appeared to be longer. To confirm this observation, we measured the aspect ratio and counted the number of pseudopodia in multiple cell samples (Fig. 2e-f). The statistical analysis showed that FDSCs had a higher aspect ratio than ADSCs and exhibited fewer pseudopodia.

Differential gene expression analysis

The functional differences between cells are driven by variations in gene expression. To further understand the functional and gene expression differences between FDSCs and ADSCs, we collected FDSCs and ADSCs from five different sample sources, resulting in a total of ten cell samples. These samples were subjected to RNA-seq and subsequent visualization analysis. Transcriptomic analysis revealed significant differences in gene expression between ADSCs and FDSCs. The heatmap of differentially expressed genes (Fig. 3a) clearly demonstrates the distinct transcriptional profiles of the two cell types. Further volcano plot analysis (Fig. 3b) showed that, compared to ADSCs, 301 genes were significantly upregulated and 174 genes were downregulated in FDSCs, indicating extensive transcriptional reprogramming in FDSCs. We also ranked all differentially expressed genes by expression level and selected the top 20 highly expressed genes for further analysis. Clustering analysis of these top 20 genes (Fig. 3c) showed that their functions were mainly enriched in developmental processes, hemoproteins, and immune regulation.

To understand the biological functions of these differentially expressed genes, we conducted Gene Ontology (GO) analysis (Fig. 3d). The results indicated that these genes were primarily enriched in pathways such as the endothelial cell apoptotic process, positive regulation of angiogenesis, and positive regulation of vasculature development. These enriched pathways suggest that FDSCs may play a critical role in regulating endothelial cell function and promoting tissue repair. The clustering characteristics of these genes further highlight the potential role of FDSCs in development and immune regulation.

To explore potential protein interactions during the vascularization process, we performed a protein-protein interaction (PPI) network prediction analysis of genes related to vascularization (Fig. 3e). The PPI network results revealed that the HMOX1 protein was prominently positioned at the center of the network,

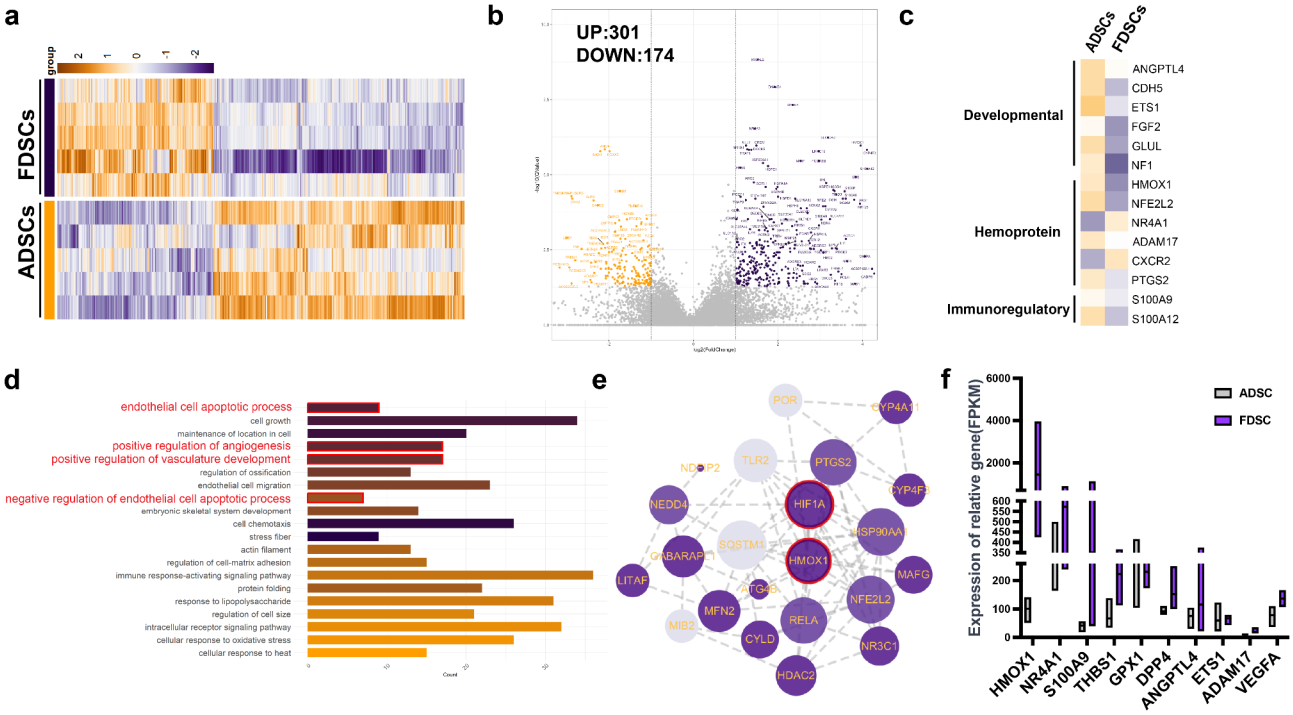

Fig. 3 Comparative transcriptomic analysis of FDSCs and ADSCs. (**a**) RNA-seq of FDSCs and ADSCs. Heatmap of global gene expression profile ($n = 5$). (**b**) Volcano plot of differential gene expression of FDSCs compared to ADSCs. (**c**) Clustering analysis of the top 20 genes with the highest expression levels. (**d**) GO analysis of differentially expressed genes highlighting enriched pathways. (**e**) Predicted key proteins identified through PPI network analysis of differentially expressed genes. (**f**) Bar chart of relevant gene expression levels (FPKM)

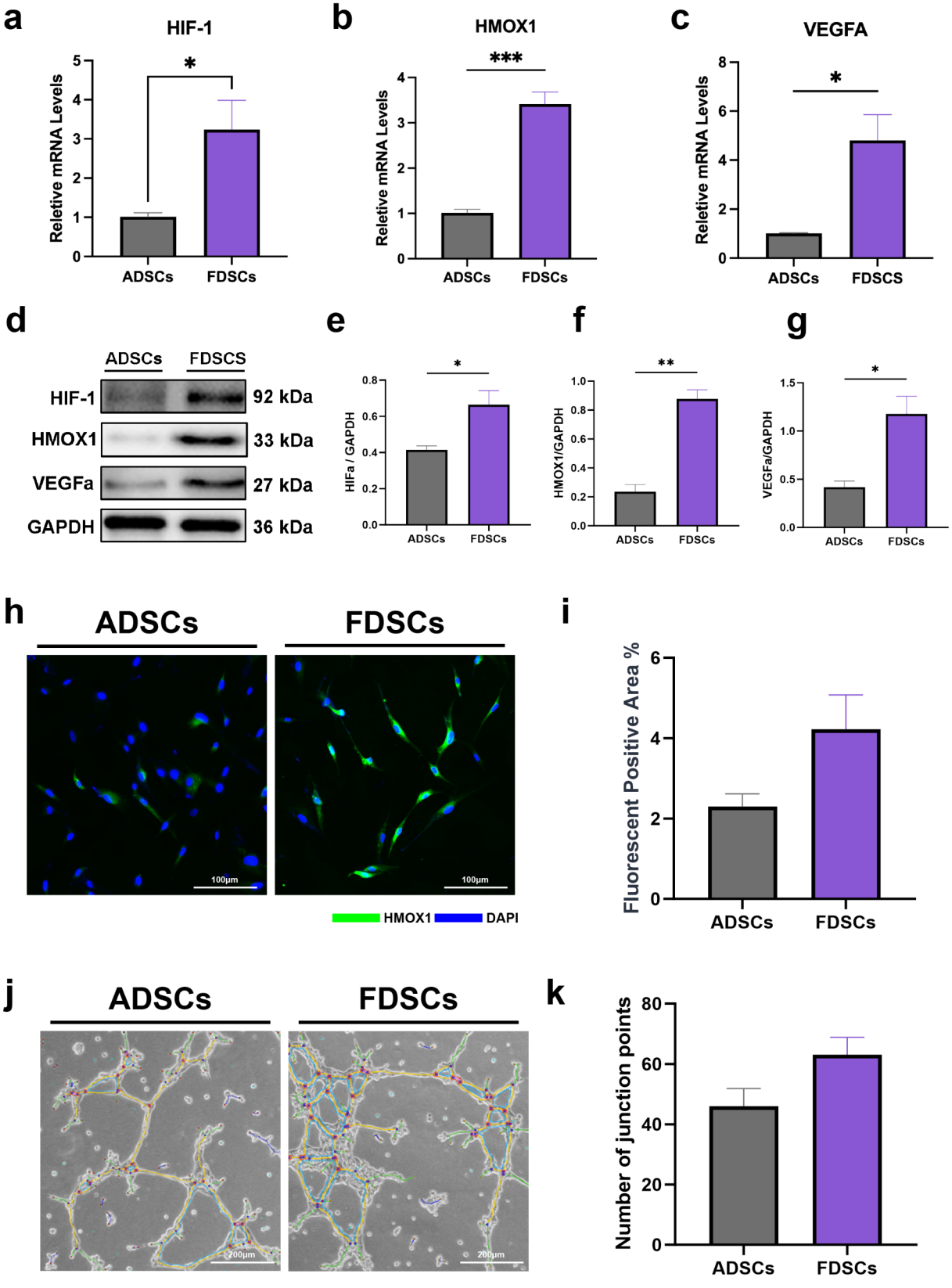

Fig. 4 (See legend on next page.)

(See figure on previous page.)

Fig. 4 Gene expression and functional assays in ADSCs and FDSCs. (**a-c**) RT-qPCR of ADSCs or FDSCs, for HIF1a, HMOX1, and VEGFa ($n=3$). (**d**). HIF1a, HMOX1 and VEGFa protein expression by Western blotting, Full-length blots/gels are presented in Supplementary Fig. 2. (**e-g**). Western blot analysis data for HIF-1α, HMOX1, and VEGF are presented as mean ± SEM of the densitometric values ($n=3$). Statistical significance was determined using two-way ANOVA (**h**) Immunofluorescence staining of HMOX1 (green) in FDSCs and ADSCs. (**i**) Quantification of HMOX1 fluorescent positive area. (**j**) Tube formation assay: Effects of FDSCs and ADSCs on endothelial tube formation. (**k**) Quantification of junction points was performed using ImageJ software. Data are presented as mean ± SEM ($n=3$)

emphasizing its role as a key regulatory hub. HMOX1 formed highly interconnected interaction patterns with several downstream effector proteins, such as HIF1A, RELA, and NFE2L2, suggesting that HMOX1 may play a central role in regulating angiogenesis and cellular stress responses. Lastly, to more intuitively display the expression differences of angiogenesis-related genes between FDSCs and ADSCs, we generated a bar chart based on the expression values of the enriched genes (Fig. 3f). The bar chart clearly shows that the expression levels of genes such as HMOX1, VEGFA, and ANGPTL4 are significantly higher in FDSCs than in ADSCs, further supporting the crucial role of FDSCs in promoting angiogenesis.

FDSCs promote angiogenesis in vitro

To validate the results of our visualization analysis, we first conducted a statistical analysis of the expression levels of HMOX1, VEGFA, and HIF1A in the transcriptomic data of FDSCs and ADSCs (see supplementary Fig. 1). The results demonstrated that the expression of these three genes differed significantly between the two cell types, further supporting our hypothesis that FDSCs possess a greater potential to promote angiogenesis. Then we conducted qPCR experiments. The results (Fig. 4a-c) showed that the average expression level of HMOX1 in FDSCs was approximately 3.4 times higher than in ADSCs, with significant statistical relevance ($p<0.001$). The expression of HIF-1 in FDSCs was around 2.9 times higher, and VEGFa expression was approximately 4.8 times higher compared to ADSCs, both with statistical significance ($p<0.05$).

Next, Western blot analysis similarly confirmed that the protein expression levels of HMOX1, HIF-1, and VEGFa were significantly higher in FDSCs than in ADSCs (Fig. 4d). After repeating the Western blot experiments three times, we observed consistent results (Fig. 4e-g). Additionally, immunofluorescence staining (Fig. 4h-i) further revealed a visibly higher expression of HMOX1 in FDSCs compared to ADSCs.

To investigate whether FDSCs can promote angiogenesis, we designed an in vitro angiogenesis assay (Fig. 4j) and quantified the number of junction points (Fig. 4k). The results showed that, at the same time point, FDSCs significantly induced more junction points in endothelial cells compared to ADSCs.

HMOX1 regulates the expression of HIF-1α and VEGFa

Previous studies have shown that HIF-1α is the primary intracellular regulator under hypoxic conditions. It stabilizes during hypoxia, translocates to the nucleus, and forms the HIF-1 complex, which activates the expression of a series of hypoxia-responsive genes, including HMOX1 and VEGF. To investigate the interaction of these three genes in FDSCs, we performed Western blot experiments. First, we examined the expression of HMOX1, HIF-1α, and VEGFa in both FDSCs and ADSCs under different durations of hypoxia. As shown in Fig. 5a, the expression of HMOX1, HIF-1α, and VEGFa increased significantly over time in both FDSCs and ADSCs, consistent with previous studies. However, when comparing the results between ADSCs and FDSCs, we observed that the expression of these three genes was consistently higher in FDSCs at all time points. This conclusion was further confirmed by quantifying grayscale values using ImageJ (Fig. 5b).

To validate these findings at the cellular level, we conducted immunofluorescence staining for HMOX1 and VEGFa. As shown in Fig. 5c, the number of VEGFa + and HMOX1 + cells increased significantly in both ADSCs and FDSCs as hypoxia duration extended, but FDSCs exhibited a markedly higher number of positive cells compared to ADSCs at the same time points. This observation was further supported by counting the number of positive cells in fields under the same magnification (Fig. 5d).

To explore the interaction between HMOX1, HIF-1α, and VEGFa, we treated FDSCs, and ADSCs after 48 h of hypoxia, with the HMOX1 inducer CP-312 (Cardioprotectant 312) and the inhibitor SnPPIX (Tin-protoporphyrin IX dichloride). Figure 5e and f show that inhibiting HMOX1 significantly reduced VEGFa expression in both cell types, consistent with the conclusion that HMOX1 acts as an upstream regulator of VEGFa.

Next, we investigated the relationship between HMOX1 and HIF1a. Interestingly, we found that inhibiting HMOX1 also led to a substantial decrease in HIF1a expression, suggesting a positive correlation between these two proteins. This was further supported by grayscale ratio analysis (Fig. 5g).

To further confirm the regulatory relationship, we treated ADSCs with the HMOX1 inducer CP-312 and examined the effects on HIF1a and VEGFa expression. As shown in Fig. 5h, CP-312 treatment significantly

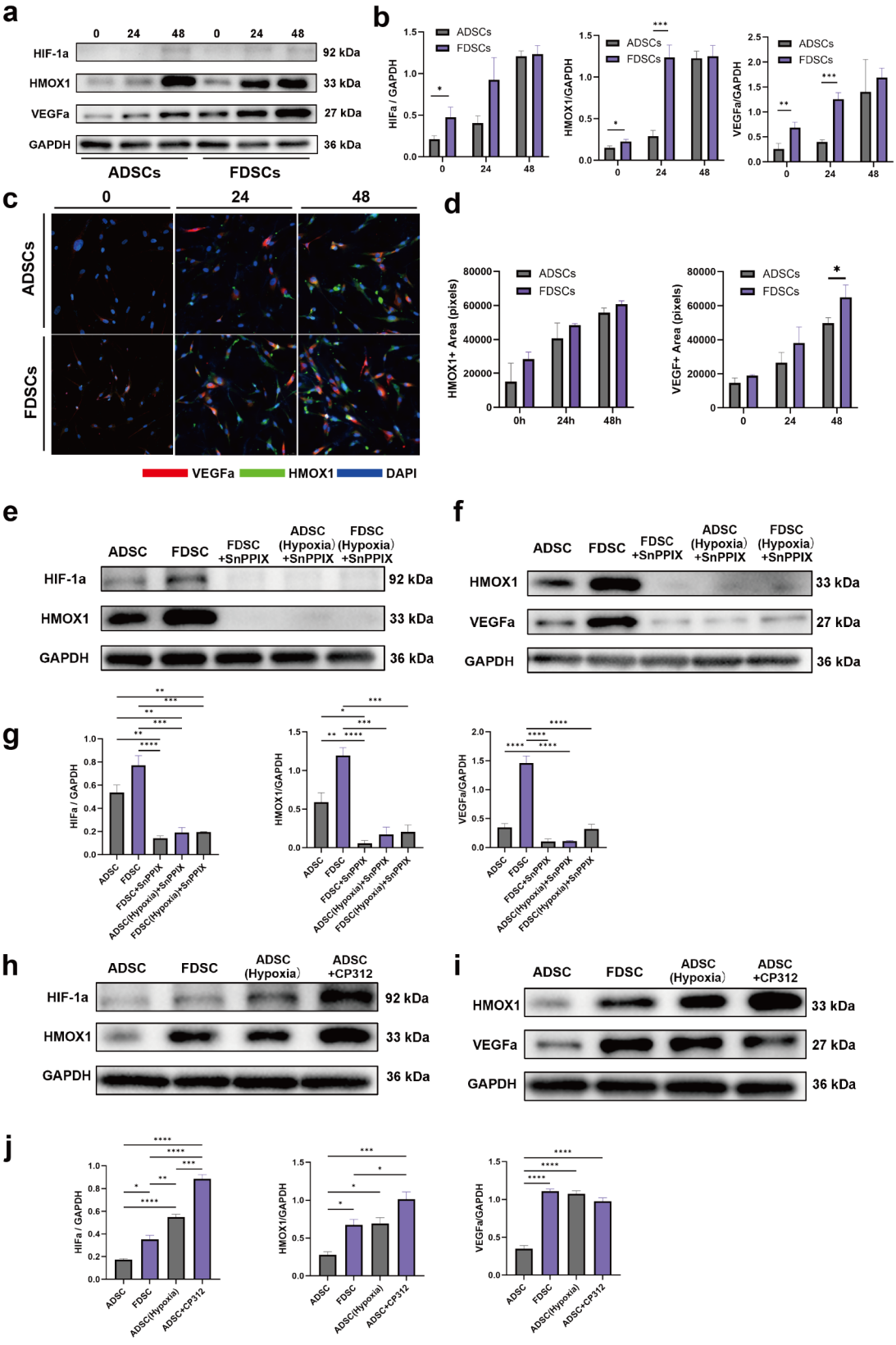

Fig. 5 (See legend on next page.)

(See figure on previous page.)

Fig. 5 Analysis of gene interactions in FDSCs and ADSCs. (**a**). HIF1a, HMOX1 and VEGFa protein expression by Western blotting. Full-length blots/gels are presented in Supplementary Fig. 3. (**b**). Western blot analysis data of HIF-1α, HMOX1, and VEGF are presented as mean ± SEM. $n = 3$, analyzed by two-way ANOVA. (**c**) Immunofluorescence staining of VEGFα (red) and HMOX1 (green) in FDSCs and ADSCs. (**d**) Quantification of VEGFα and HMOX1 fluorescent positive area. (**e-f**). Western blot analysis of HIF1α, HMOX1, and VEGFa protein expression in FDSCs and ADSCs following SnPPIX treatment. Full-length blots/gels are presented in Supplementary Figs. 4–5. (**g**). Western blot data of HIF-1α, HMOX1, and VEGF after SnPPIX treatment, presented as mean ± SEM ($n = 3$), analyzed by two-way ANOVA. (**h-i**) Western blot analysis of HIF1α, HMOX1, and VEGFa protein expression in FDSCs and ADSCs following CP312 treatment. Full-length blots/gels are presented in Supplementary Figs. 6–7. (**j**). Western blot data of HIF-1α, HMOX1, and VEGF after CP312 treatment, presented as mean ± SEM ($n = 3$), analyzed by two-way ANOVA

increased HMOX1 expression, accompanied by a rise in VEGFa levels. Although VEGFa expression under CP-312 treatment was lower than in hypoxic conditions, it remained higher than in normoxic ADSCs, further proving that HMOX1 regulates VEGFa expression. Similarly, we observed an increase in HIF1a expression alongside the upregulation of HMOX1, reinforcing the positive correlation between HMOX1 and HIF1a. Grayscale ratio analysis (Fig. 5j) further confirmed this conclusion.

HMOX1 Knockdown reduces HIF-1α and VEGFa expression and impairs angiogenesis

To further investigate the upstream and downstream relationship between HMOX1 and HIF-1α, we used lentiviral-mediated knockdown of HMOX1 in FDSCs and ADSCs to analyze its impact on the expression levels of HIF-1α and VEGFa, as well as its effect on angiogenic functionality. Since the lentiviral-transduced cells carried GFP markers, we first assessed the efficiency of HMOX1 knockdown by observing the expression of green fluorescence. As shown in Fig. 6a, all cells exhibited green fluorescence, confirming successful HMOX1 knockdown in FDSCs and ADSCs.

Subsequently, we analyzed gene and protein expression levels using qPCR and Western blot. The results demonstrated that HMOX1 knockdown significantly reduced HIF-1α and VEGFa expression levels in both FDSCs and ADSCs (Fig. 6b–f). This finding aligns with the regulatory relationship shown in Fig. 5, further confirming that HMOX1 regulates VEGFa expression by modulating HIF-1α stability.

To clarify the role of HIF-1α in this process, we treated HMOX1-knockdown cells with the HIF-1α activator FG-4592. The results showed that FG-4592 partially restored VEGFa expression levels (Fig. 6b–f), validating that HIF-1α mediates the downstream regulatory effect of HMOX1 on VEGFa.

For functional validation, we used the conditioned media from HMOX1-knockdown FDSCs and HMOX1-knockdown ADSCs cultured under hypoxic conditions to treat endothelial cells. The results revealed that endothelial tube-forming ability was significantly impaired within 2 h (Fig. 6g–h). This functional alteration corresponded with the decreased VEGFa levels, further emphasizing the critical role of the HMOX1-HIF-1α-VEGFa axis in maintaining the angiogenic microenvironment.

FDSC co-transplantation enhances graft retention and vascularization

To investigate whether FDSCs can promote graft retention and vascularization in vivo, we mixed the obtained FDSCs and ADSCs with fat and transplanted 0.5 ml of the mixture into the dorsal region of nude mice (method). Samples were collected on days 7, 14, and 30 to assess graft outcomes. Gross examination of the harvested grafts revealed that the FDSC co-transplantation group had more extensive microvascular coverage on the graft surface compared to the ADSC group (Fig. 7a).

When analyzing graft retention rates, we found that the FDSC co-transplantation group consistently showed higher retention rates than the ADSC group at all time points—days 7, 14, and 30 (Fig. 7b). To assess graft viability, we performed HE staining on the graft sections. On day 30, the FDSC group exhibited a greater number of viable adipocytes, fewer oil cysts, less inflammatory cell infiltration, and reduced fibrosis compared to the ADSC group (Fig. 7c).

To evaluate vascularization, we performed CD31 immunofluorescence staining (Fig. 7d). The results demonstrated that, on day 30, the number of CD31 + endothelial cells in the FDSC group was significantly higher than in the ADSC group. Quantification of the red fluorescent area across different samples revealed a similar trend (Fig. 7e).

Lastly, to explore the relationship between HMOX1 and VEGF, we performed immunofluorescence staining on the collected samples at various time points, labeling HMOX1 in green and VEGF in red (Fig. 7f). The results indicated that VEGF fluorescence increased over time in both the FDSC and ADSC groups. However, HMOX1 expression was significantly higher in the FDSC group. Quantitative analysis of multiple samples confirmed this finding (Fig. 7g-h).

Discussion

As a widely distributed connective tissue in the human body, fascia not only provides physical support to adipose tissue but also plays a key role in fat metabolism, storage, and distribution [18]. While the relationship between fascia and adipose tissue is well recognized [19, 20], the characteristics and specific roles of Fascia-Derived Stem Cells (FDSCs) under physiological and pathological conditions remain unclear. In this study, we systematically

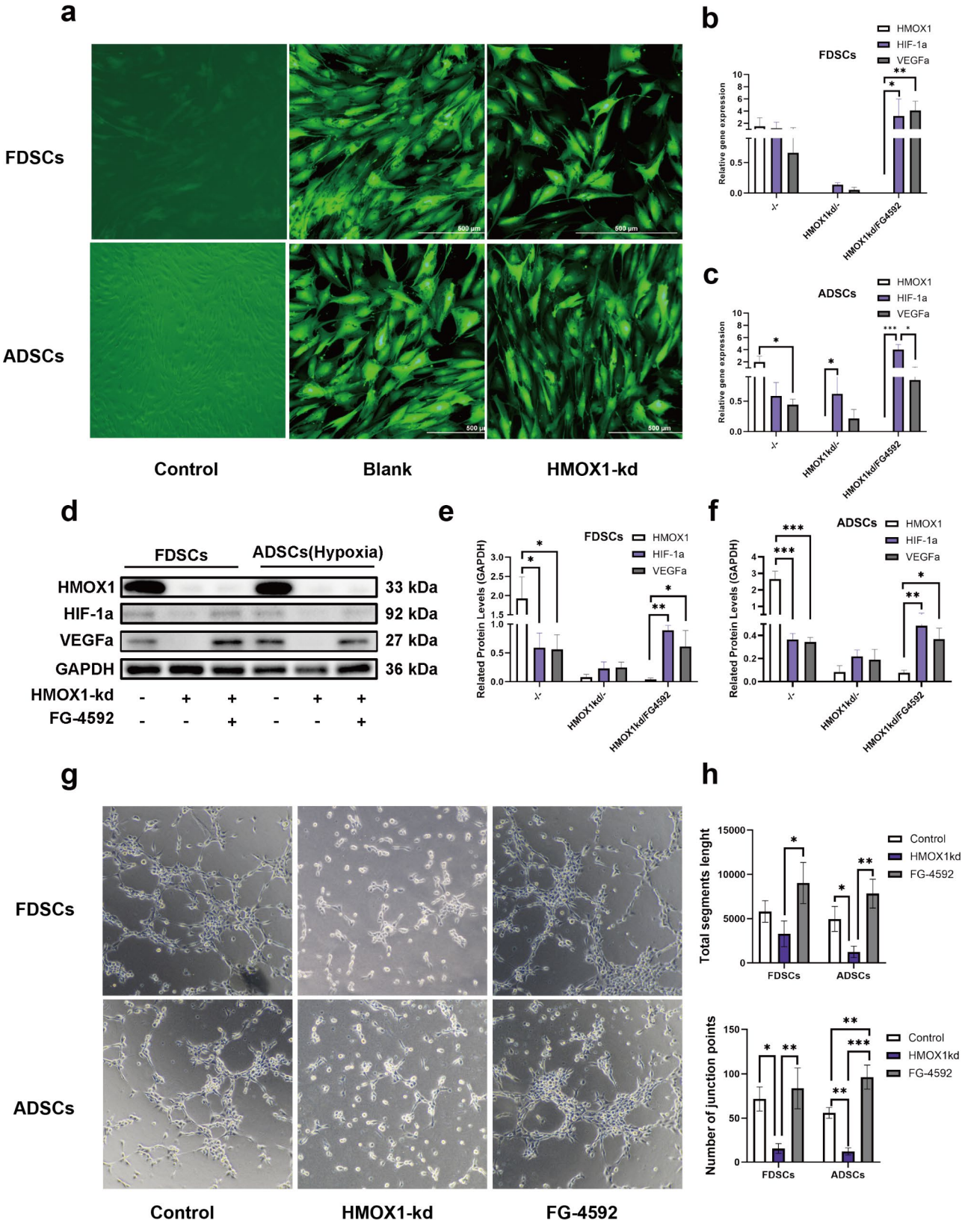

Fig. 6 (See legend on next page.)

(See figure on previous page.)

Fig. 6 HMOX1 knockdown in FDSCs and ADSCs impairs angiogenic functionality. (**a**) Efficiency of HMOX1 knockdown in FDSCs and ADSCs was assessed via GFP expression, indicating successful lentiviral transduction. Scale bars: 500 μm. (**b**–**c**) Quantitative real-time PCR (qPCR) analysis of HMOX1, HIF-1α, and VEGFa mRNA levels in FDSCs (**b**) and ADSCs (**c**) with or without HMOX1 knockdown, as indicated. Data are normalized to GAPDH and presented as mean ± SEM ($n = 3$). (**d**) Western blot analysis of HMOX1, HIF-1α, and VEGFa expression under normoxic conditions in FDSCs and under hypoxic conditions in ADSCs. Comparisons are shown between control, HMOX1-knockdown cells, and HMOX1-knockdown cells treated with the HIF-1α activator FG-4592. GAPDH served as the loading control. Full-length blots/gels are presented in Supplementary Fig. 8. (**e**–**f**) Densitometric quantification of Western blot bands for HMOX1, HIF-1α, and VEGFa relative to GAPDH, presented as mean ± SEM ($n = 3$). Statistical significance was determined by two-way ANOVA. (**g**) Representative phase-contrast images of tube formation by endothelial cells incubated with conditioned media derived from FDSCs and ADSCs under control conditions, following HMOX1 knockdown, and after HMOX1 knockdown with FG-4592 treatment. Images were captured at 2 h. (**h**) Quantification of total segment length and the number of junction points from the tube formation assay, performed using ImageJ software. Data are presented as mean ± SEM ($n = 3$). Statistical significance was evaluated by ANOVA, with $^{*}p < 0.05$, $^{**}p < 0.01$, and $^{***}p < 0.001$

describe the cytological and functional characteristics of FDSCs and conduct a comparative analysis with adipose-derived mesenchymal stem cells (ADSCs). Our results show that FDSCs, while originating from distinct anatomical locations, also express multiple stem cell surface markers. Additionally, FDSCs display significant differences in gene expression patterns compared to ADSCs. In an in vivo fat transplantation model, FDSCs significantly enhance graft survival and retention by promoting angiogenesis. These findings suggest that FDSCs may play an important role in adipose tissue repair and regeneration, offering potential clinical applications in fat transplantation and tissue regeneration.

In the comparative analysis of the cytological and functional characteristics of FDSCs and ADSCs, we first analyzed third-passage cells for mesenchymal stem cell-specific markers, including CD34, SCA-1, and CD29, and evaluated their trilineage differentiation potential [21, 22]. The results confirmed that these cells exhibit typical mesenchymal stem cell characteristics, demonstrating their multipotency and differentiation capabilities. Notably, in our adipogenic differentiation experiments, we observed that FDSCs exhibit weaker adipogenic potential compared to ADSCs. Similar findings were reported in the study by Hing-Lok Wong et al. [23], which demonstrated that while FDSCs have a relatively lower adipogenic capacity, their chondrogenic potential is stronger than that of ADSCs. This difference may be attributed to the tissue origin of FDSCs, as fascia is a collagen-rich structure, similar to cartilage in composition, than a fat storage tissue. Consequently, the adipogenic capacity of FDSCs may be constrained by these structural characteristics. On the other hand, Naoki Ishiuchi et al. [24] provided an alternative explanation, suggesting that the lower adipogenic capacity of FDSCs could be related to differences in the expression of genes involved in cell cycle and division, such as CENPF, BUB1B, and ANLN. Additionally, other studies [25] have proposed that stem cells derived from fascia express higher levels of fibrosis-related genes, such as TGFB, and fibrosis and adipogenesis are biologically opposing processes. These varying hypotheses highlight the current lack of a unified explanation for the reduced adipogenic potential of FDSCs, and further research is needed to elucidate this mechanism. Nonetheless, it appears that lower adipogenic capacity is a characteristic feature of fascia-derived stem cells. To ensure the accuracy of our findings, we used flow cytometry to exclude interference from fibroblasts, leukocytes, and endothelial cells during cell identification, focusing on the markers FAP, CD45, and CD31. FFAP, a transmembrane glycoprotein, is mainly expressed in activated fibroblasts and is closely associated with fibrotic potential [26]. It promotes fibroblast phenotype changes by regulating key signaling molecules such as MMPs, thereby affecting the fibrotic process. Thus, determining FAP expression effectively excludes fibroblasts. CD45, a specific leukocyte marker, is broadly expressed across all leukocytes and serves as a key marker for identifying immune cells [27]. Using CD45 helps eliminate immune cells, allowing for more precise analysis of non-immune cells. CD31, a specific endothelial marker, is crucial in vascular biology and helps identify vascular endothelial cells [28]. Our analysis showed that the cells we examined expressed minimal levels of FAP, CD45, and CD31, indicating they were not fibroblasts, immune cells, or endothelial cells. This confirms the purity of the mesenchymal stem cell population used in our study.

In our morphological analysis, we used phalloidin staining to examine the cytoskeleton and found that FDSCs had a significantly greater aspect ratio compared to ADSCs. In studies on the relationship between stem cell morphology and function, cells with larger spreading areas and more adhesion points tend to have smaller aspect ratios, which confers higher survival potential, particularly in adverse environments such as hypoxia. In contrast, spindle-shaped cells with larger aspect ratios, like FDSCs, tend to exhibit greater sensitivity to environmental changes and may possess enhanced migratory capacity under stress conditions [29]. These morphological differences suggest important biological functional distinctions between FDSCs and ADSCs.

To further explore the functional differences and potential mechanisms between FDSCs and ADSCs, we conducted transcriptome sequencing analysis. This aimed to uncover differences in gene expression and

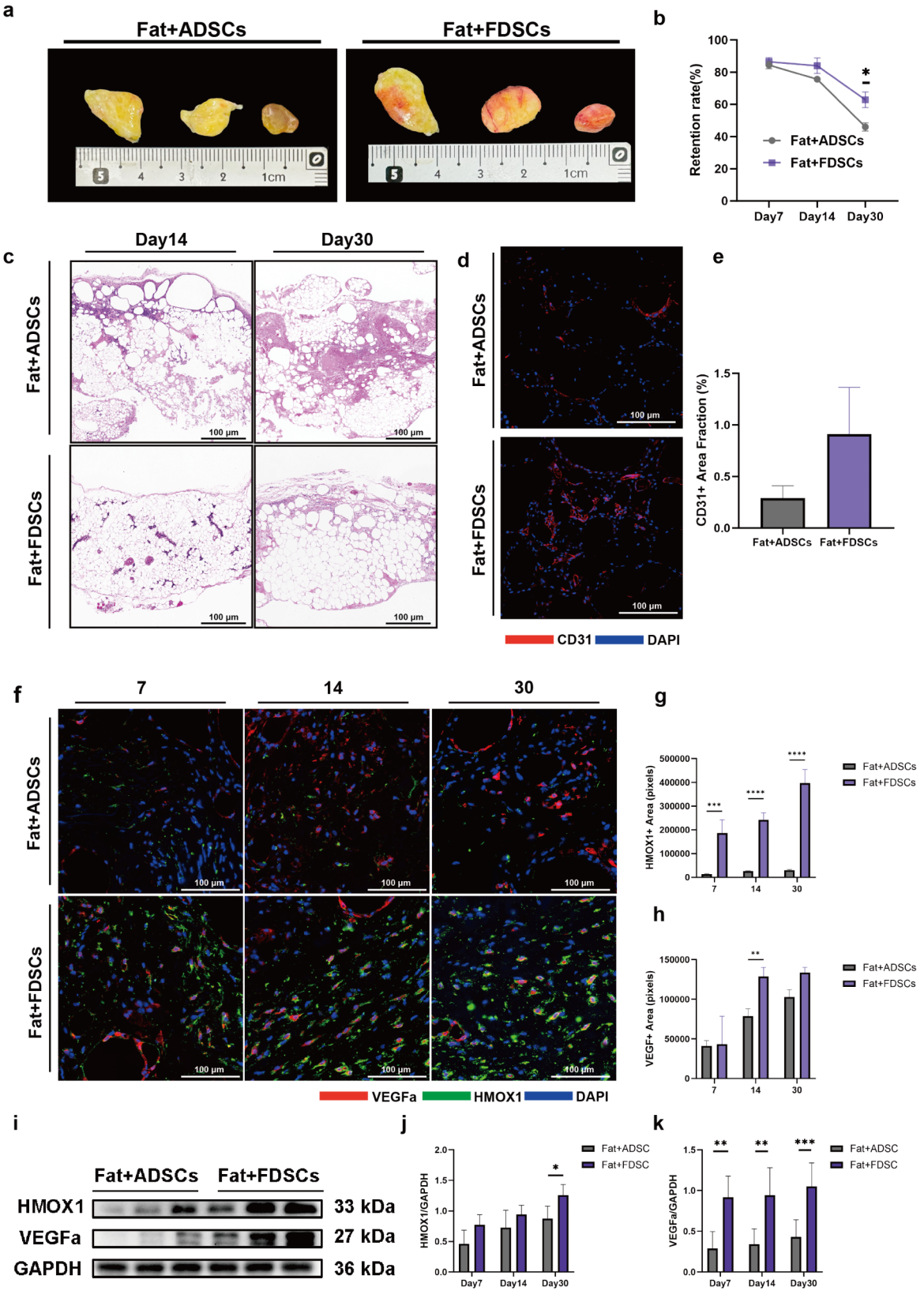

Fig. 7 (See legend on next page.)

(See figure on previous page.)

Fig. 7 Co-transplantation of FDSCs with adipose tissue enhances graft retention and vascularization. (**a**) Macroscopic view of grafts at days 7, 14, and 30, from left to right. (**b**). Line graph of graft volume over time. (**c**). H&E staining of grafts. (**d**). Immunofluorescence staining of CD31, with CD31 in red and DAPI in blue. (**e**). Quantification of the CD31 + fluorescent area. (**f**). Immunofluorescence images of HMOX1 (green) and VEGFa (red), with DAPI in blue. (**g-h**). Quantification of VEGF + and HMOX1 + fluorescent areas. (**i**) Western blot analysis of HMOX1 and VEGFa protein expression in grafts at different time points. Full-length blots/gels are presented in Supplementary Fig. 9. (**j-k**) Densitometric quantification of Western blot bands for HMOX1 and VEGFa relative to GAPDH, presented as mean ± SEM ($n = 3$). Statistical significance was determined by two-way ANOVA

provide insights into their unique functional characteristics and adaptive responses.

Through the visualization of sequencing results, we found that compared to ADSCs, FDSCs exhibited 301 upregulated genes and 174 downregulated genes, indicating distinct gene expression patterns between the two cell types. To gain deeper insights into the functional implications of these differentially expressed genes, we conducted Gene Ontology (GO) analysis. The results revealed that these genes were primarily enriched in biological processes such as endothelial cell development and cell growth, strongly suggesting that FDSCs may play a key role in maintaining and regulating endothelial cell activity and function.

We then performed clustering analysis on the top 20 genes with the greatest differential expression. The results showed that these genes were mainly associated with functions such as developmental processes and hemoprotein regulation. This gene regulation pattern highlights FDSCs' unique advantage in promoting angiogenesis. Additionally, through protein-protein interaction (PPI) network prediction analysis, we identified HMOX1 as a central protein in the network, underscoring its pivotal regulatory role in angiogenesis and cellular stress responses.

Notably, several genes associated with hypoxia response and angiogenesis were significantly upregulated in FDSCs, including HIF-1α, HMOX1, NR4A1, ETS1, and VEGFa. Given that HIF-1α was also identified as a central node in the PPI network prediction analysis, we focused our attention on this gene. HIF-1α is a transcription factor first described by Gregg L. Semenza and colleagues while investigating the regulatory mechanisms of erythropoietin (EPO), including HIF-1α and HIF-1β [30]. Specifically, HIF-1α, as a key transcription factor under hypoxic conditions, stabilizes in low-oxygen environments and translocates to the nucleus, where it binds with HIF-1β to form a functional transcription factor complex. This complex activates the expression of angiogenesis-related genes, including VEGF, to promote the formation of new blood vessels [31].

Interestingly, research has shown that after the HIF-1 complex binds to the hypoxia response element (HRE), it recruits transcriptional co-activators, such as p300 and CBP. These co-activators enhance the expression of downstream genes like HMOX1 by acetylating histones, further promoting angiogenesis.

HMOX1 encodes the enzyme heme oxygenase-1 (HO-1), which catalyzes the breakdown of heme into iron, carbon monoxide (CO), and biliverdin. This process helps degrade excess heme to prevent its potential toxicity, while also regulating inflammatory and oxidative stress responses. Additionally, HMOX1 plays a key role in promoting vascularization. As a stress-induced enzyme, it degrades heme into CO, ferrous iron (Fe^{2+}), and biliverdin, with biliverdin exerting anti-inflammatory effects by inhibiting the production and release of pro-inflammatory cytokines, such as TNF-α, IL-1β, and IL-6. This reduction in inflammation alleviates its detrimental effects on endothelial cells and enhances VEGF expression, further promoting angiogenesis.

Subsequently, through qPCR, Western blot, and immunofluorescence experiments, we further validated the expression of these genes at both the transcriptome and protein levels, supporting the reliability of our sequencing results. Finally, the tube formation assay results demonstrated that FDSCs significantly promoted endothelial cell tubule formation compared to ADSCs, further confirming the effectiveness of FDSCs in promoting angiogenesis. This finding provides strong support for utilizing the vascularization potential of FDSCs to enhance graft retention in subsequent animal studies.

Notably, the Western blot experiments not only verified the expression of relevant genes in FDSCs but also, through the use of the HMOX1 inducer CP-312 [32] and inhibitor SnPPIX [16], revealed the dual regulatory role of HMOX1. Specifically, our experiments showed that HMOX1 not only regulates VEGFa expression but also has a positive correlation with HIF-1α expression. While most studies suggest that HIF-1α acts as an upstream factor of HMOX1, stabilizing and activating under hypoxic conditions and directly binding to the hypoxia response element (HRE) in the HMOX1 promoter region to promote its transcription—a well-established regulatory pathway—our research suggests that HMOX1 also has the potential to positively regulate HIF-1α, influencing its stability and function through a different mechanism [33] (Fig. 8).

Louise L. Dunn and her colleagues' research also supports this view [14]. They found that carbon monoxide (CO), produced during the heme degradation process by HMOX1, can directly stabilize HIF-1α and prevent its rapid degradation. Therefore, we hypothesize that the mechanism by which HMOX1 regulates HIF-1α involves

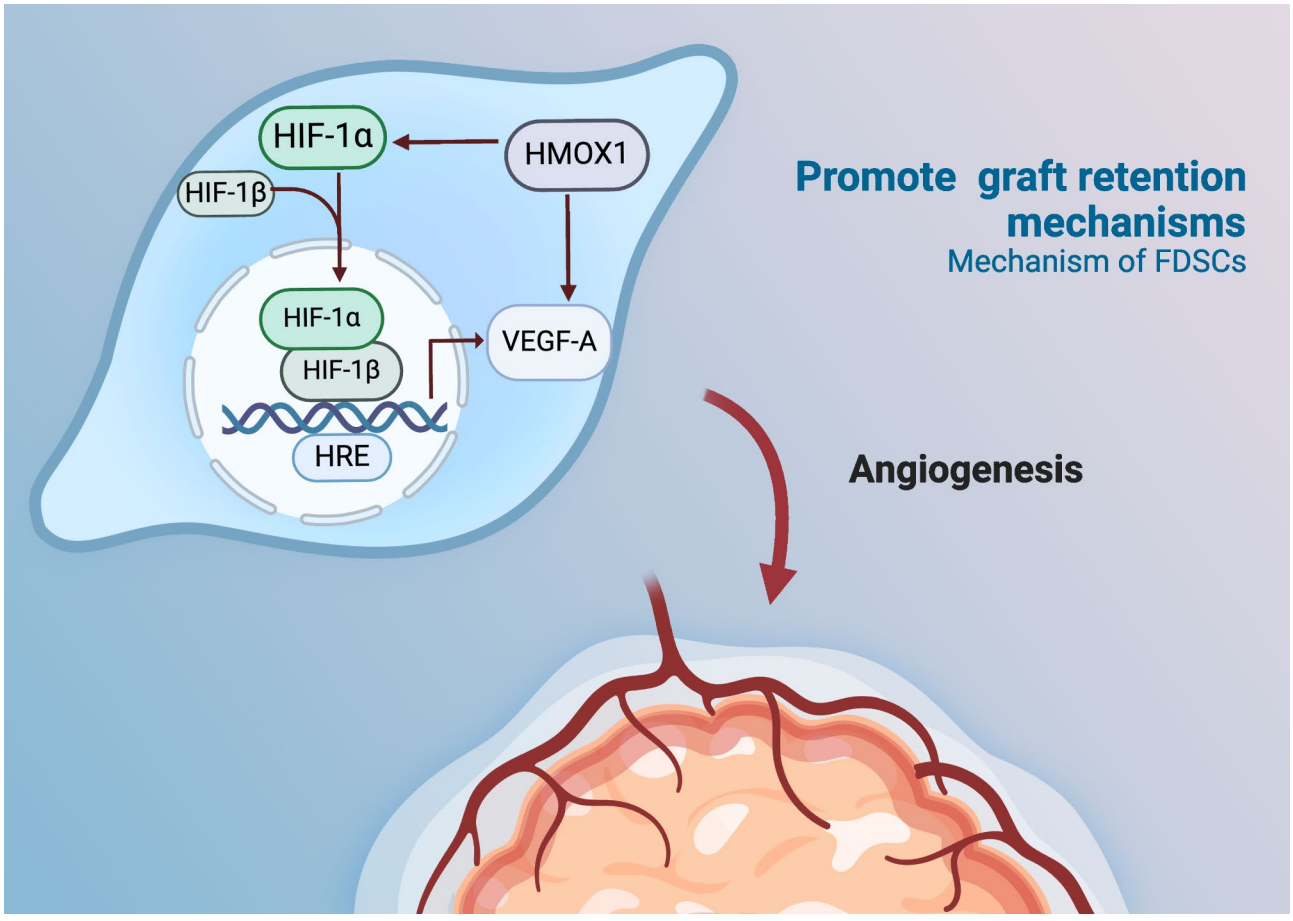

Fig. 8 Schematic representation of FDSC mechanism of action

CO acting as a critical signaling molecule in the regulation of HIF-1α [34].

The PHD (prolyl hydroxylase) family, particularly PHD2, is a key enzyme responsible for the hydroxylation of HIF-1α [35]. PHDs add hydroxyl groups to specific sites on HIF-1α (such as P402 and P564), marking it for recognition and degradation by the ubiquitin-proteasome pathway. Under normoxic conditions, PHDs are active, promoting the rapid degradation of HIF-1α and maintaining low intracellular levels of HIF-1α. However, under hypoxic or oxidative stress conditions, the activity of PHD2 is inhibited, allowing HIF-1α to accumulate and function as a transcription factor.

In the context of high HMOX1 expression, the increase in CO binds to cytochrome aa3 in the mitochondria, promoting the production of more H_2O_2. H_2O_2 facilitates the formation of PHD2 dimers through disulfide bonds, and these dimers exhibit lower enzymatic activity compared to their monomeric forms. Specifically, H_2O_2 modulates the dimerization state of PHD2, reducing its hydroxylation of HIF-1α and thereby inhibiting the degradation of HIF-1α [36]. This results in a significant increase in the stability and expression levels of HIF-1α. Consequently, H_2O_2 indirectly promotes the accumulation and functional activity of HIF-1α by inhibiting the activity of PHD2.

Therefore, HMOX1 stabilizes and enhances the expression of HIF-1α by producing CO, which in turn increases the levels of H_2O_2, leading to the inhibition of PHD2 activity. However, this unconventional mechanism of HIF-1α stabilization still requires further investigation.

In summary, our study not only uncovers the molecular mechanisms by which FDSCs regulate HIF-1α and VEGF expression through HMOX1 under hypoxic conditions but also provides theoretical support for early angiogenesis following fat transplantation. Given the potential advantages of FDSCs in promoting vascularization and improving the hypoxic microenvironment, we further explored their potential application in fat transplantation.

After fat transplantation, the graft often remains in a hypoxic and nutrient-deficient state due to incomplete integration with the host's blood supply [37]. This unfavorable microenvironment leads to the rapid death of various cells, including adipocytes, resulting in a high rate of necrosis and resorption following fat transplantation. However, under hypoxic conditions, stem cells

surrounding the graft are activated and secrete a range of pro-angiogenic factors and chemokines, rapidly promoting the formation of new blood vessels and improving the hypoxic state [38]. This process is crucial for the early survival of ischemic fat grafts. Consequently, the addition of stem cells to grafts, a strategy known as cellassisted lipotransfer (CAL), has emerged as an effective approach [39].

Although ADSCs are commonly used to support traditional fat transplantation, this method still faces challenges of insufficient vascularization and suboptimal graft quality [40]. Given our findings that FDSCs exhibit significant advantages in promoting angiogenesis, we explored the potential of FDSCs to enhance vascularization in fat transplantation. By comparing grafts supplemented with FDSCs to those with ADSCs, we found that FDSCs significantly improved early post-transplant survival rates, structural integrity of adipose tissue, and density of newly formed blood vessels. These results were further confirmed by HE staining and CD31 immunofluorescence imaging.

Additionally, we focused on the role of the HMOX1 gene in FDSC-mediated angiogenesis. By co-staining for HMOX1 and VEGF and performing immunofluorescence staining on graft samples at different time points, we revealed a strong positive correlation between HMOX1 and VEGF. This finding also corroborated the results from our Western blot experiments.

Overall, this discovery not only highlights the potential of FDSCs in fat transplantation but also points to a potential mechanism in which HMOX1-high FDSCs promote angiogenesis in stem cell-assisted transplantation therapies.

In conclusion, the superficial fascia is widely distributed throughout the body and serves as an important source of mesenchymal stem cells. Similar to stem cells derived from other tissues, FDSCs from the superficial fascia exhibit great potential in tissue engineering, particularly in areas such as wound healing and aesthetic surgery. As an alternative therapeutic approach, FDSCs show promising prospects, especially due to their strong angiogenic capabilities. Given these advantages, further research will help optimize their clinical applications, providing more effective solutions for tissue repair and regeneration. However, it is important to acknowledge that due to the limited availability of human specimens and the necessity of obtaining donor consent, we were unable to isolate FDSCs from distinct anatomical locations in this study. In future research, we will explore FDSCs from various anatomical sites to further understand their diverse properties.

Conclusion

Our study demonstrates that fascia-derived stem cells (FDSCs) possess distinct characteristics and offer significant advantages in promoting angiogenesis compared to adipose-derived stem cells (ADSCs). Through a combination of transcriptome analysis, functional assays, and in vivo experiments, we confirmed that FDSCs exhibit enhanced angiogenic capabilities, which are likely regulated by the HMOX1-HIF-1α-VEGF signaling pathway. The ability of FDSCs to improve graft survival and retention, particularly in hypoxic environments, highlights their potential as a promising therapeutic tool in fat transplantation and tissue regeneration. Further research into the mechanisms underlying their reduced adipogenic capacity and their strong pro-angiogenic function will help optimize their clinical applications for more effective tissue repair and regeneration strategies.

Abbreviations

FDSCs	Fascia-derived stem cells
ADSCs	Adipose-derived stem cells
HIF-1α	Hypoxia-inducible factor-1α
HMOX1	Heme oxygenase-1
MSCs	Mesenchymal stem cells
PPARγ	Peroxisome Proliferator-Activated Receptor Gamma
C/EBPα	CCAAT/Enhancer Binding Protein Alpha
TGF-β	Transforming Growth Factor Betavascular endothelial growth factor
CO	Carbon monoxide
PBS	Phosphate-buffered saline
DMEM	Dulbecco's Modified Eagle Medium
RUNX2	Runt-Related Transcription Factor 2
BMP-2	Bone Morphogenetic Protein 2
SOX9	SRY-Box Transcription Factor 9
qPCR	Quantitative real-time polymerase chain reaction
DEGs	Differentially Expressed Genes
HUVECs	Human Umbilical Vein Endothelial Cells
SVF	Stromal vascular fraction

Supplementary Information

The online version contains supplementary material available at https://doi.org/10.1186/s13287-025-04204-w.

Supplementary Material 1

Supplementary Material 2

Supplementary Material 3

Supplementary Material 4

Supplementary Material 5

Supplementary Material 6

Supplementary Material 7

Supplementary Material 8

Supplementary Material 9

Supplementary Material 10

Acknowledgements

Thank you to the staff of the Laboratory Animal Center of the Fourth Military Medical University for their dedicated care of the experimental animals.

Author contributions
Guo Chen, Jie Long, Yuge Zhang, Xuhua Zhou, Botao Gao, Zijin Qin Yuhan Zhu, Binyu Song, Ziwei Cui, Zhangzi liu, Man Xu performed the all experiments. Guo Chen, Jie Long and Ziang Zhang wrote the paper. Guo Chen, Yuge Zhang, Xuhua Zhou, Botao Gao performed cell experiments and prepared figures. Guo Chen did the statistical analyses. Guo Chen performed animal experiments. Ziang Zhang, Zhou Yu and Baoqiang Song conceived and designed the experiments and reviewed drafts of the paper. Ziang Zhang, Zhou Yu and Baoqiang Song contributed to reagents and materials.

Funding
This work was supported by grants from the National Natural Science Foundation of China under Grant 82102355.

Data availability
All data relevant to the study are included in the article or uploaded as supplemental file 1.

Declarations

Ethics approval and consent to participate
All animal experiments were conducted in accordance with the protocol approved by the Fourth Military Medical University Laboratory Animal Welfare and Ethics Committee (IACUC-20241434). The date of approval is May 1, 2024 The title of the approved project is: Fascia-Derived Stem Cells Enhance Fat Graft Retention by Promoting Vascularization through the HMOX1-HIF-1α Pathway. The use of human samples and the experimental protocol in this study were approved by the Medical Ethics Committee of the First Affiliated Hospital of the Air Force Medical University (Approval Number: KY20222104-F-2, Title: "The Role of Human-Derived Stem Cells in Promoting Angiogenesis in Fat Grafting"). The date of approval is October 18, 2022.

Consent for publication
Not applicable.

Competing interests
The authors declare that they have no known competing financial interests or personal relationships that could have appeared to influence the work reported in this paper.
The authors declare that they have not use AI-generated work in this manuscript.

Author details
[1]Department of Plastic and Reconstruction Surgery, Xijing Hospital, Fourth Military Medical University, Xi'an, Shaanxi, China
[2]Department of Medical Cosmetic Center, Affiliated Hangzhou First People's Hospital, School of Medicine, Westlake University, 310006 Hangzhou, Zhejiang, China
[3]Department of Craniomaxillofacial Surgery, Plastic Surgery Hospital, Chinese Academy of Medical Science and Peking Union Medical College, Beijing, China

Received: 3 October 2024 / Accepted: 29 January 2025
Published online: 25 February 2025

References

1. Denadai R, Raposo-Amaral CA, Raposo-Amaral CE. Fat Grafting in managing Craniofacial deformities. Plast Reconstr Surg. 2019;143(5):1447–55. https://doi.org/10.1097/PRS.0000000000005555.
2. Wang Z, Huang M, Zhang Y, et al. Comparison of Biological properties and clinical application of mesenchymal stem cells from the mesoderm and ectoderm. STEM CELLS INT. 2023;2023(4547875). https://doi.org/10.1155/2023/4547875.
3. Haga CL, Booker CN, Carvalho A, Boregowda SV, Phinney DG. Transcriptional targets of TWIST1 in human mesenchymal Stem/Stromal cells mechanistically Link Stem/Progenitor and paracrine functions. Stem Cells. 2023;41(12):1185–200. https://doi.org/10.1093/stmcls/sxad070.
4. Vincentz JW, Firulli BA, Lin A, Spicer DB, Howard MJ, Firulli AB. Twist1 controls a cell-specification switch governing cell fate decisions within the cardiac neural crest. PLoS Genet. 2013;9(3):e1003405. https://doi.org/10.1371/journal.pgen.1003405.
5. Baptista LS, Côrtes I, Montenegro B et al. A novel conjunctive microenvironment derived from human subcutaneous adipose tissue contributes to physiology of its superficial layer. Stem Cell Res Ther. 2021;12(1):480. Published 2021 Aug 28. https://doi.org/10.1186/s13287-021-02554-9
6. Zhang Y, Su X, Dong Y, et al. Cytological and functional characteristics of fascia adipocytes in rats: a unique population of adipocytes. Biochim Biophys Acta Mol Cell Biol Lipids. 2020;1865(2):158585. https://doi.org/10.1016/j.bbalip.2019.158585.
7. Merrick D, Sakers A, Irgebay Z, et al. Identification of a mesenchymal progenitor cell hierarchy in adipose tissue. Science. 2019;364(6438):eaav2501. https://doi.org/10.1126/science.aav2501.
8. Su X, Lyu Y, Wang W, et al. Fascia Origin of Adipose cells. Stem Cells. 2016;34(5):1407–19. https://doi.org/10.1002/stem.2338.
9. Choi MY, Kim HI, Yang YI, et al. The isolation and in situ identification of MSCs residing in loose connective tissues using a niche-preserving organ culture system. Biomaterials. 2012;33(18):4469–79. https://doi.org/10.1016/j.biomaterials.2012.03.009.
10. Rehnke RD. Clinical Implications of the Fascial System: A Commentary on One Surgeon's Journey. Life (Basel). 2024;14(1):89. Published 2024 Jan 5. https://doi.org/10.3390/life14010089
11. Mizuno H, Tobita M, Uysal AC. Concise review: adipose-derived stem cells as a novel tool for future regenerative medicine. Stem Cells. 2012;30(5):804–10. https://doi.org/10.1002/stem.1076.
12. Lee HJ, Ryu JM, Jung YH, Oh SY, Lee SJ, Han HJ. Novel pathway for Hypoxia-Induced Proliferation and Migration in Human mesenchymal stem cells: involvement of HIF-1α, FASN, and mTORC1. Stem Cells. 2015;33(7):2182–95. https://doi.org/10.1002/stem.2020.
13. Dulak J, Łoboda A, Zagórska A, Józkowicz A. Complex role of heme oxygenase-1 in angiogenesis. Antioxid Redox Signal. 2004;6(5):858–66. https://doi.org/10.1089/ars.2004.6.858.
14. Dunn LL, Kong SMY, Tumanov S, et al. Hmox1 (Heme Oxygenase-1) protects against ischemia-mediated Injury via stabilization of HIF-1α (hypoxia-Inducible Factor-1α). Arterioscler Thromb Vasc Biol. 2021;41(1):317–30. https://doi.org/10.1161/ATVBAHA.120.315393.
15. Kirby RJ, Divlianska DB, Whig K et al. Discovery of Novel Small-Molecule Inducers of Heme Oxygenase-1 That Protect Human iPSC-Derived Cardiomyocytes from Oxidative Stress [published correction appears in J Pharmacol Exp Ther. 2018;364(2):179. doi: 10.1124/jpet.117.243717err]. J Pharmacol Exp Ther. 2018;364(1):87–96. https://doi.org/10.1124/jpet.117.243717
16. Abdalla MY, Ahmad IM, Rachagani S, et al. Enhancing responsiveness of pancreatic cancer cells to gemcitabine treatment under hypoxia by heme oxygenase-1 inhibition. Transl Res. 2019;207:56–69. https://doi.org/10.1016/j.trsl.2018.12.008.
17. Wang J, Xin Lv, Aniwan A, et al. O-GlcNAcylation regulates HIF-1α and induces mesothelial-mesenchymal transition and fibrosis of human peritoneal mesothelial cells. Heliyon. 2023;9(12):e22916. https://doi.org/10.1016/j.heliyon.2023.e22916. Published 2023 Dec 1.
18. Cenaj O, Allison DHR, Imam R, et al. Evidence for continuity of interstitial spaces across tissue and organ boundaries in humans. Commun Biol. 2021;4(1):436. https://doi.org/10.1038/s42003-021-01962-0. Published 2021 Mar 31.
19. Bi X, Li B, Zou J, et al. Fascia promotes adipose tissue regeneration by improving early macrophage infiltration after Fat Grafting in a mouse model. Plast Reconstr Surg. 2023;152(3):e446–57. https://doi.org/10.1097/PRS.0000000000010259.
20. Ziegler ME, Sorensen AM, Banyard DA, et al. Deconstructing allograft adipose and Fascia Matrix: Fascia Matrix improves angiogenesis, volume Retention, and adipogenesis in a Rodent Model. Plast Reconstr Surg. 2023;151(1):108–17. https://doi.org/10.1097/PRS.0000000000009794.
21. Dang J, Yang J, Yu Z, et al. Bone marrow mesenchymal stem cells enhance angiogenesis and promote fat retention in fat grafting via polarized macrophages. Stem Cell Res Ther. 2022;13(1):52. https://doi.org/10.1186/s13287-022-02709-2. Published 2022 Feb 4.
22. Li H, Ghazanfari R, Zacharaki D, Lim HC, Scheding S. Isolation and characterization of primary bone marrow mesenchymal stromal cells. Ann N Y Acad Sci. 2016;1370(1):109–18. https://doi.org/10.1111/nyas.13102.
23. Wong HL, Siu WS, Fung CH, Zhang C, Shum WT, Zhou XL, Lau CB, Zhang JF, Leung PC, Fu WM, Ko CH. Characteristics of stem cells derived from rat fascia: in vitro proliferative and multilineage potential assessment. Mol Med Rep.

2015;11(3):1982–90. https://doi.org/10.3892/mmr.2014.2967. Epub 2014 Nov 18. PMID: 25405325.
24. Ishiuchi N, Nakashima A, Maeda S, Miura Y, Miyasako K, Sasaki K, Uchiki T, Sasaki A, Nagamatsu S, Nakao N, Nagao M, Masaki T. Comparison of therapeutic effects of mesenchymal stem cells derived from superficial and deep subcutaneous adipose tissues. Stem Cell Res Ther. 2023;14(1):121. https://doi.org/10.1186/s13287-023-03350-3. PMID: 37143086; PMCID: PMC10161523.
25. Estève D, Boulet N, Belles C, Zakaroff-Girard A, Decaunes P, Briot A, Veeranagouda Y, Didier M, Remaury A, Guillemot JC, Ledoux S, Dani C, Bouloumié A, Galitzky J. Lobular architecture of human adipose tissue defines the niche and fate of progenitor cells. Nat Commun. 2019;10(1):2549. https://doi.org/10.1038/s41467-019-09992-3. PMID: 31186409; PMCID: PMC6560121.
26. Su S, Chen J, Yao H, et al. CD10 + GPR77 + Cancer-Associated fibroblasts promote Cancer formation and chemoresistance by sustaining Cancer Stemness. Cell. 2018;172(4):841–e85616. https://doi.org/10.1016/j.cell.2018.01.009.
27. Trowbridge IS, Thomas ML. CD45: an emerging role as a protein tyrosine phosphatase required for lymphocyte activation and development. Annu Rev Immunol. 1994;12:85–116. https://doi.org/10.1146/annurev.iy.12.040194.000505.
28. Newman PJ, Berndt MC, Gorski J, et al. PECAM-1 (CD31) cloning and relation to adhesion molecules of the immunoglobulin gene superfamily. Science. 1990;247(4947):1219–22. https://doi.org/10.1126/science.1690453.
29. Mathieu PS, Loboa EG. Cytoskeletal and focal adhesion influences on mesenchymal stem cell shape, mechanical properties, and differentiation down osteogenic, adipogenic, and chondrogenic pathways. Tissue Eng Part B Rev. 2012;18(6):436–44. https://doi.org/10.1089/ten.TEB.2012.0014.
30. Semenza GL, Agani F, Booth G, et al. Structural and functional analysis of hypoxia-inducible factor 1. Kidney Int. 1997;51(2):553–5. https://doi.org/10.1038/ki.1997.77.
31. Ziello JE, Jovin IS, Huang Y. Hypoxia-inducible factor (HIF)-1 regulatory pathway and its potential for therapeutic intervention in malignancy and ischemia. Yale J Biol Med. 2007;80(2):51–60.
32. Kirby RJ, Divlianska DB, Whig K et al. Discovery of Novel Small-Molecule Inducers of Heme Oxygenase-1 That Protect Human iPSC-Derived Cardiomyocytes from Oxidative Stress [published correction appears in J Pharmacol Exp Ther. 2018;364(2):179. https://doi.org/10.1124/jpet.117.243717err]. J Pharmacol Exp Ther. 2018;364(1):87–96. doi:10.1124/jpet.117.243717.
33. Ayer A, Zarjou A, Agarwal A, Stocker R. Heme Oxygenases in Cardiovascular Health and Disease. Physiol Rev. 2016;96(4):1449–508. https://doi.org/10.1152/physrev.00003.2016.
34. Chin BY, Jiang G, Wegiel B, et al. Hypoxia-inducible factor 1alpha stabilization by carbon monoxide results in cytoprotective preconditioning. Proc Natl Acad Sci U S A. 2007;104(12):5109–14. https://doi.org/10.1073/pnas.0609611104.
35. Jaakkola P, Mole DR, Tian YM, et al. Targeting of HIF-alpha to the Von Hippel-Lindau ubiquitylation complex by O2-regulated prolyl hydroxylation. Science. 2001;292(5516):468–72. https://doi.org/10.1126/science.1059796.
36. Lee G, Won HS, Lee YM, et al. Oxidative dimerization of PHD2 is responsible for its inactivation and contributes to metabolic reprogramming via HIF-1α activation. Sci Rep. 2016;6:18928. https://doi.org/10.1038/srep18928. Published 2016 Jan 7.
37. Mashiko T, Yoshimura K. How does fat survive and remodel after grafting? Clin Plast Surg. 2015;42(2):181–90. https://doi.org/10.1016/j.cps.2014.12.008.
38. Rehman J, Traktuev D, Li J, et al. Secretion of angiogenic and antiapoptotic factors by human adipose stromal cells. Circulation. 2004;109(10):1292–8. https://doi.org/10.1161/01.CIR.0000121425.42966.F1.
39. Yoshimura K, Sato K, Aoi N, Kurita M, Hirohi T, Harii K. Cell-assisted Lipotransfer for Cosmetic breast augmentation: supportive use of adipose-derived Stem/Stromal cells. Aesthetic Plast Surg. 2020;44(4):1258–65. https://doi.org/10.1007/s00266-020-01819-7.
40. Si Z, Wang X, Sun C, et al. Adipose-derived stem cells: sources, potency, and implications for regenerative therapies. Biomed Pharmacother. 2019;114:108765. https://doi.org/10.1016/j.biopha.2019.108765.

Publisher's note

Springer Nature remains neutral with regard to jurisdictional claims in published maps and institutional affiliations.